

Topology of the Flow around a Conventional Submarine Hull

S.-K. Lee^{1,2}

¹Defence Science and Technology Organisation, Melbourne, VIC 3207 AUSTRALIA

²University of Tasmania, Launceston, TAS 7250 AUSTRALIA

Abstract

A topology model constructed from surface-streamer visualisation describes the flow of a generic conventional Defence Science and Technology Organisation (DSTO) submarine design in straight-ahead and yaw conditions. The model is used to derive equations for the side-force and yaw-moment coefficients relating to the geometry of the hull and the circulation of the surrounding flow.

Introduction

Tests of submarine hulls at DSTO make use of a generic conventional hull shape defined by Joubert [1]. The design objectives of this shape are to provide “minimum practical resistance with minimum water flow noise... while still carrying out all its normal functions” [1]. The resistance depends on geometric parameters such as the slenderness ratio of the hull, and the location and height of the fin. The flow noise is in part due to fluid-structure interaction, and since this contributes to the acoustic signature of the hull, it is useful to gain some understanding of the (vortex) structure of the flow.

Figure 1 shows the shape defined by Joubert, where the slenderness ratio for the bare hull is 7.3 to minimise resistance [1]. The shape of the nose is based on a NACA-0014.2-N00.20 profile and is axisymmetric for the first 7% of the body length (L_{oa}). Tapering to the end of the tail cone begins at 76% L_{oa} . The fin has the shape of a NACA-0015 aerofoil but with a rounded trailing edge; the fin height is 8% L_{oa} , the chord length is 16% L_{oa} and the leading edge is located at 31% L_{oa} . The aft control surfaces are “X”-rudders located at 86-91% L_{oa} .

For prediction of manoeuvrability it is necessary to estimate the hydrodynamic forces and moments. Due to the complexity of geometry, the forces are usually estimated on a part-by-part basis: starting with the hull, then adding appendage force(s) and the propulsion. As submarines typically have small appendages, the normal-force distributed over the hull is a substantial contribution to the total force and moment.

This paper examines flows over the hull and the fin since these produce the flow (vortex) structure which most affect the distribution of forces and moments. Only the structure of separated flow produced by yaw is considered here.

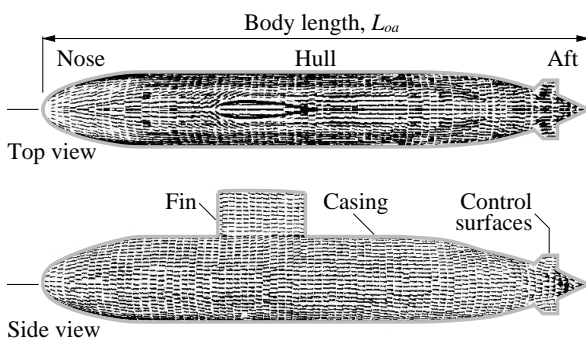


Figure 1. DSTO submarine, time-averaged (stable) flow; $\psi = 0$.

Surface-Streamer Visualisation

Evidence of surface-flow separation is obtained by attaching streamers on a model of the hull ($L_{oa} = 1.35$ m). The streamers are woolen threads 10-mm long and 1-mm in diameter. Motion of the streamers is observed in the air flow of the closed-circuit, low-speed wind tunnel at DSTO. The test section of the tunnel is 2.74-m wide \times 2.13-m high. The hull is supported on a turntable. Streamer-flow images are obtained for yaw angles (ψ) of 0, 10 and 18°. Images shown here are ensemble averages of 125 frames from a video camera at 25 frames/second with the background subtracted to isolate the streamers. Resolution of the images is 1 mm/pixel. The Reynolds number based on body length and the free-stream velocity ($Re_L = L_{oa}U_{\infty}/\nu = 4.5 \times 10^6$) is sufficiently large that details of the flow are not sensitive to small changes in Reynolds number.

Interpretation of the Surface Flow

At zero yaw, the flow is symmetrical about the mirror plane of the submarine (Fig. 1). The flow pattern is stable and there is no large-scale separation along the hull. In Fig. 2, the surface streaklines obtained from interpretation of the streamer visualisation begin at an attachment node (N_n) on the nose and terminate at a separation node (N_a) aft of the hull. The junction flow produced by the fin includes a stagnation node-and-saddle (N_{fj} , S_{fj}) pair and a “U-shaped” negative bifurcation (NB_c). On the casing, a positive-bifurcation (PB_c) line runs between the legs of the U-shaped negative bifurcation (NB_c).

At 10° yaw, the flow is no longer symmetrical (Fig. 3). Since the surface of the hull is continuous in the circumferential direction, Fig. 4 shows that the flow spreading from both the windward side (positive bifurcation PB_{hw}) and the leeward side (positive bifurcation PB_{hl}) converges on the upper hull (negative bifurcations NB_{hc} and NB_c) and on the lower hull (negative bifurcation NB_{hb}), thus satisfying continuity. On the leeward side of the fin, a streak of fluctuating streamers indicates strong turbulence and separation. In Fig. 4, this feature is shown as a negative-bifurcation (NB_{fl}) line.

At 18° yaw, the positive bifurcations (PB_{hw} and PB_{hl}) are stronger and there is stronger turbulence over a larger area on the leeward side of the fin (Fig. 5). In instantaneous images and in the video recording, streamers radiate from a point on the leeward surface of the fin, implying that there is a reattach-

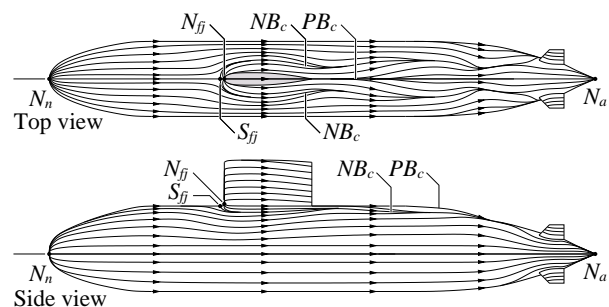


Figure 2. Surface-streakline interpretation of Fig. 1.

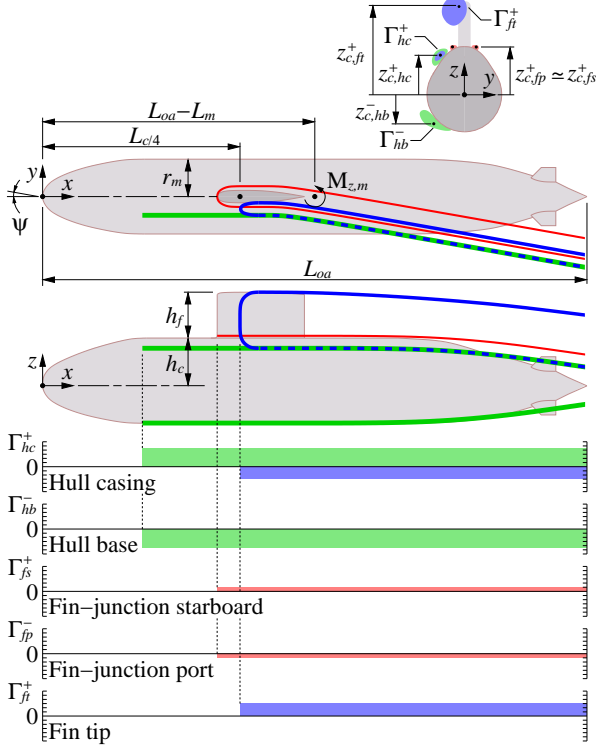


Figure 7. Schematic diagram of instantaneous vortex lines and the distribution of circulation around the submarine, $\Sigma\Gamma(x) = 0$.

scale with the displacement thickness of the boundary layer ($\delta^* \simeq 1.7x/\sqrt{Re_L} \sim L_{oa}/1000$), are comparably smaller than the hull vortices and the fin-tip vortex. As the fin-junction vortices on the casing are part of the same horseshoe vortex, this gives $\Gamma_{fs}^+ + \Gamma_{fp}^- = 0$ and $\Gamma_{fs}^+ z_{c,fs}^+ + \Gamma_{fp}^- z_{c,fp}^- \simeq 0$, and so Eqs. (5) and (6) may be simplified to

$$\Sigma\Gamma(x) = \Gamma_{hc}^+ + \Gamma_{hb}^- + \Gamma_{ft}^+ = 0, \quad (7)$$

$$g_{y,h}(x) = \Gamma_{hc}^+ z_{c,hc}^+ + \Gamma_{hb}^- z_{c,hb}^- + \Gamma_{ft}^+ z_{c,ft}^+. \quad (8)$$

Force on the Hull

Jeans et al. [2] have shown that, for a slender hull at incidence (angle ψ) operating at a large Reynolds number ($Re_L \gtrsim 10^6$), the force distribution (force per unit length) parallel to the cross-stream (y) direction is

$$\frac{d}{dx} F_{y,h}(x) = \rho U_{\infty x} \frac{d}{dx} i_{y,h}(x), \quad (9)$$

where ρ is the fluid density, $U_{\infty x} = U_{\infty} \cos(\psi)$ is the body-axis velocity and $i_{y,h}(x)$ is known as the hydrodynamic impulse per unit length parallel to the y direction [2]:

$$i_{y,h}(x) = g_{y,h}(x) - U_{\infty y} A_h(x), \quad (10)$$

which depends on the moment of vorticity $g_{y,h}(x)$ and the local cross-section area of the hull $A_h(x)$. Integrating Eq. (9) gives

$$F_{y,h} = \rho U_{\infty x} \int_0^{L_{oa}} di_{y,h}(x) = \rho U_{\infty} \cos(\psi) \times g_{y,h,\text{aft}}, \quad (11)$$

where $g_{y,h,\text{aft}} = i_{y,h,\text{aft}}$ since $A_{h,\text{aft}} = 0$; the subscript ‘‘aft’’ denotes measurement at the tail plane ($x = L_{oa}$). Substituting Eqs. (2), (4) and (8) into Eq. (11) yields

$$F_{y,h} = \rho U_{\infty}^2 r_m \cos(\psi) \sin(\psi) \times \left(\kappa_{hc}^+ z_{c,hc,\text{aft}}^+ + \kappa_{hb}^- z_{c,hb,\text{aft}}^- + \kappa_{ft}^+ z_{c,ft,\text{aft}}^+ \right). \quad (12)$$

From integration (by parts) of the moment of Eq. (9) over the body length, this gives the yaw moment about the tail plane [2]:

$$M_{z,h,\text{aft}} = \rho U_{\infty x} \int_0^{L_{oa}} i_{y,h}(x) dx. \quad (13)$$

To obtain the yaw moment about the mid-ship, Eq. (13) may be recast as

$$M_{z,h,m} = K_h \times F_{y,h} L_m, \quad (14)$$

where L_m is the distance from the tail plane to the mid-ship of the hull and K_h is a coefficient of proportionality.

Force on the (NACA-0015) Fin

The simplest interpretation of the flow around the fin is the superposition of the free-stream and a U-shaped vortex (Fig. 7). This U-shaped vortex (line) consists of three segments: (i) a bound vortex which spans along the height of the fin about the hydrodynamic centre of the fin, connected to (ii) a vortex leg along the tip of the fin and (iii) a vortex leg along the casing. In reality, there would be infinitely many instantaneous (U-shaped-like) vortex lines spread along the fin, forming a wake with local strength $\Gamma_{fb}(z)$. The side force acting on the fin is

$$F_{y,f} = \rho U_{\infty} \int_{h_c}^{h_c+h_f} \Gamma_{fb}(z) dz, \quad (15)$$

where h_c is the height of the casing and h_f is the height of the fin measured from the casing (see Fig. 7). By the Helmholtz vortex law, circulation produced by the fin-bound vortex is equal to the circulation of the fin-tip vortex:

$$\Gamma_{fb} = \Gamma_{ft}, \quad (16)$$

and so Eq. (15) may be recast as

$$F_{y,f} = K_f \times \rho U_{\infty} \Gamma_{ft}^+ h_f, \quad (17)$$

where K_f is a coefficient of proportionality. By substituting Eq. (4) into Eq. (17), this gives the force acting on the hydrodynamic centre of the fin:

$$F_{y,f} = \rho U_{\infty}^2 r_m \sin(\psi) \times K_f \kappa_{ft}^+ h_f. \quad (18)$$

The mid-ship yaw moment due to this force is given by

$$M_{z,f,m} = F_{y,f} \times \left(L_{oa} - L_m - L_{c/4} \right), \quad (19)$$

where $L_{c/4} < L_{oa} - L_m$ is the distance from the nose to the quarter-chord point of the fin (Fig. 7).

Force on the Overall Geometry

By adding Eqs. (12) and (18), this gives the total side force:

$$F_y = \rho U_{\infty}^2 r_m \sin(\psi) \times \left[K_1 \cos(\psi) + K_f K_2 \right] L_{oa} \quad (20)$$

and by adding Eqs. (14) and (19), this gives the total yaw moment about the mid-ship:

$$M_{z,m} = \rho U_{\infty}^2 r_m \sin(\psi) \times \left[\frac{L_m}{L_{oa}} K_h K_1 \cos(\psi) + \left(1 - \frac{L_m}{L_{oa}} - \frac{L_{c/4}}{L_{oa}} \right) K_f K_2 \right] L_{oa}^2, \quad (21)$$

where

$$K_1 = \kappa_{hc}^+ \frac{z_{c,hc,\text{aft}}^+}{L_{oa}} + \kappa_{hb}^- \frac{z_{c,hb,\text{aft}}^-}{L_{oa}} + \kappa_{ft}^+ \frac{z_{c,ft,\text{aft}}^+}{L_{oa}}, \quad (22)$$

$$K_2 = \kappa_{ft}^+ \frac{h_f}{L_{oa}}. \quad (23)$$

From Fig. 7, it is possible to infer the location of the vortices. For example, the vertical distance between the centroids of the

hull vortices does not exceed the maximum diameter of the hull:

$$\frac{z_{c,hc,aft}^+ - z_{c,hb,aft}^-}{L_{oa}} = \gamma_h \frac{1}{R}, \quad 0 < \gamma_h < 1, \quad (24)$$

and the vertical location of the tip vortex does not exceed the height of the fin:

$$\frac{z_{c,ft,aft}^+}{L_{oa}} = \gamma_f \left(\frac{1}{2R} + \frac{h_f}{L_{oa}} \right), \quad 0 < \gamma_f < 1, \quad (25)$$

where γ_h and γ_f are coefficients of proportionality for the hull vortices and the fin vortex respectively, and $R = L_{oa}/(2r_m)$ is the slenderness ratio of the hull. For a hull with an approximately round cross-section, this gives $z_{c,hc,aft}^+ \simeq -z_{c,hb,aft}^-$, and so substituting Eqs. (24) and (25) into Eq. (22) yields

$$K_1 = \gamma_h \frac{1}{2R} (\kappa_{hc}^+ - \kappa_{hb}^-) + \gamma_f \left(\frac{1}{2R} + \frac{h_f}{L_{oa}} \right) \kappa_{ft}^+, \quad (26)$$

which relates K_1 to the geometry of the submarine.

Force and Moment Coefficients

By non-dimensionalising Eqs. (20) and (21), this gives the side-force and mid-ship yaw-moment coefficients:

$$C_{F_y} = F_y / \left(\frac{1}{2} \rho U_\infty^2 L_{oa}^2 \right) = \left[\frac{K_1}{R} \cos(\psi) + \frac{K_f K_2}{R} \right] \sin(\psi), \quad (27)$$

$$C_{M_z} = M_{z,m} / \left(\frac{1}{2} \rho U_\infty^2 L_{oa}^3 \right) = \left[\frac{L_m}{L_{oa}} \frac{K_h K_1}{R} \cos(\psi) + \left(1 - \frac{L_m}{L_{oa}} - \frac{L_{c/4}}{L_{oa}} \right) \frac{K_f K_2}{R} \right] \sin(\psi). \quad (28)$$

Figure 8 shows the force and moment coefficients plotted as functions of yaw angle (ψ) for the generic conventional submarine $R = 7.3$, $L_m/L_{oa} = 1/2$, $L_{c/4}/L_{oa} = 0.35$ and $h_f/L_{oa} = 0.08$. The measurements are for $Re_L = 5.2 \times 10^6$ tested in the low-speed wind tunnel at DSTO [3]. They are obtained using a 6-component strain-gauge balance fitted inside the submarine via a single-pylon support on a turntable. The measurement uncertainties for C_{F_y} and C_{M_z} are 0.15×10^{-3} and 0.03×10^{-3} , respectively [3]. In the absence of the fin ($K_f = 0$, $K_2 = 0$ and $\kappa_{ft}^+ = 0$), the data (+) in the range $5^\circ \leq \psi \leq 15^\circ$ falls on

$$C_{F_y} = 0.042 \cos(\psi) \sin(\psi), \quad (29)$$

$$C_{M_z} = 0.017 \cos(\psi) \sin(\psi), \quad (30)$$

with r.m.s. errors of 21% and 7% respectively. Trial and error show that, for example $\gamma_h = 1/2$, Eq. (26) yields $\kappa_{hc}^+ = -\kappa_{hb}^- = K_1 R / \gamma_h = 4.5$, which agrees well with simulation result [2] for bare hulls similar to the present geometry.

For a NACA-0015 aerofoil, a review of circulation data [4] suggests $\kappa_{ft}^+ = 3$. By observing the Helmholtz vortex law (Fig. 7), this gives a prediction of the distribution of circulation when the fin is added to the hull, i.e. $\kappa_{hb}^- = -4.5$, $\kappa_{ft}^+ = 3$ and $\kappa_{hc}^+ = 1.5$, where $\Sigma \kappa = 0$ since $\Sigma \Gamma = 0$ by Eq. (7). Inspection of particle image velocimetry [5] measurements suggests that, at the tail plane of the submarine, the vertical location of the tip vortex is approximately three-quarters of the distance from the centre-line of the hull to the top of the fin, i.e. $\gamma_f = 3/4$. By substituting the values $\kappa_{hb}^- = -4.5$, $\kappa_{ft}^+ = 3$, $\kappa_{hc}^+ = 1.5$, $\gamma_h = 1/2$ and $\gamma_f = 3/4$ into Eqs. (26) and (23), this gives $K_1 = 0.540$ and $K_2 = 0.240$. By least-squares fitting to the experimental data (\diamond) in the range $5^\circ \leq \psi \leq 15^\circ$:

$$C_{F_y} = [0.074 \cos(\psi) + 0.0192] \sin(\psi), \quad (31)$$

$$C_{M_z} = [0.020 \cos(\psi) + 0.0029] \sin(\psi), \quad (32)$$

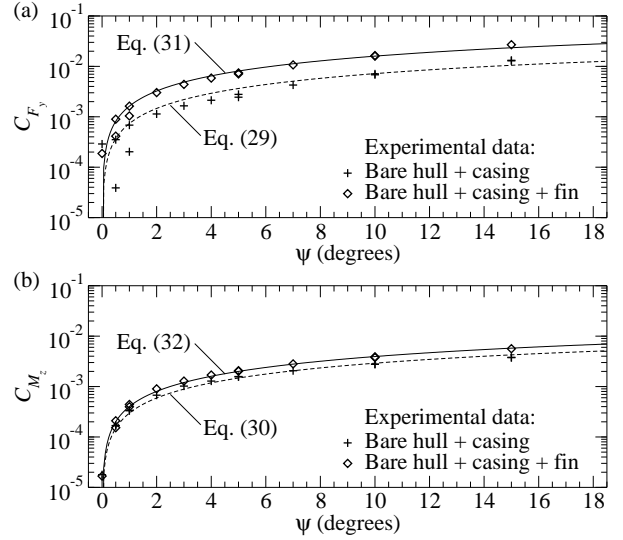


Figure 8. Force and moment coefficients for the DSTO hull form; a curve fit of Eqs. (27) and (28) on experimental data [3].

with r.m.s. errors of 9% and 3% respectively, the remaining coefficients $K_f = 0.584$ and $K_h = 0.546$ are determined.

Concluding Remarks

A topology model of the flow produced by a generic conventional submarine at yaw is presented. An analytical treatment of this model provides a first step towards equations which relate the force and moment coefficients to the submarine geometry and the circulation of the surrounding flow. Further refinement would need to take into account the effects of control surfaces, the arrangement of sting or pylon support(s), propulsion and the Reynolds number to obtain general equations. This requires more data and analysis to extend the present model.

Acknowledgements

The author offers his sincere thanks to Mr. C. Kumar for assisting with the flow-visualisation experiment, to Dr. G. Seil and Mr. P. Manovski for reviewing this paper, and to Mr. H. Quick for providing the force and moment data for the generic conventional (DSTO) submarine geometry. The support from the SEA1000 project is gratefully acknowledged.

References

- [1] Joubert, P. N. Some aspects of submarine design part 2: shape of a submarine 2026. TR1920, DSTO, 2006.
- [2] Jeans, T. L., Holloway, A. G. L., Watt, G. D. & Gerber, A. G. A force estimation method for viscous separated flow over slender axisymmetric bodies with tapered tails. *Journal of Ship Research*, 2010, 54:53–67.
- [3] Quick, H. & Woodyatt, B. Phase II experimental testing of a generic submarine model in the DSTO low speed wind tunnel. TN1274, DSTO, 2014.
- [4] Birch, D., Lee, T., Mokhtarian, F. & Kafyeke F. Structure and induced drag of a tip vortex. *Journal of Aircraft*, 2004, 41:1138–1145.
- [5] Kumar, C., Manovski, P. & Giacobello, M. Particle image velocimetry measurements on a generic submarine hull form. In *Proceedings of the 18th Australasian Fluid Mechanics Conference, Paper 188*, Launceston, Australia, 2012.